THE JOURNAL OF PHYSICAL CHEMISTRY C
A JOURNAL OF THE AMERICAN CHEMICAL SOCIETY

pubs.acs.org/JPCC

Article

Strongly and Weakly Adsorbed H_2O Layer Thicknesses on Hydroxylated SiO_2 Surfaces versus H_2O Pressure at Various Substrate Temperatures

Published as part of The Journal of Physical Chemistry C special issue "Vicki H. Grassian Festschrift".

Samantha M. Rau, Rebecca J. Hirsch, Marcel Junige, Andrew S. Cavanagh, Antonio L. P. Rotondaro, Hanna Paddubrouskaya, Kate H. Abel, and Steven M. George*

Cite This: J. Phys. Chem. C 2025, 129, 1666−1677

Read Online

ACCESS | Metrics & More | Article Recommendations | Supporting Information

ABSTRACT: The H_2O layer thickness on flat hydroxylated SiO_2 surfaces was measured at various H_2O pressures and substrate temperatures using in situ real-time spectroscopic ellipsometry (SE). The in situ SE measurements were conducted at 18.1, 27.2, and 30.4 °C (291.25, 300.35, and 303.55 K) in a warm-wall vacuum chamber designed with a cooled sample stage. The H_2O pressures were varied up to the saturation H_2O vapor pressures of 15.6, 27.0, and 32.5 Torr at 18.1, 27.2, and 30.4 °C, respectively. The SE measurements showed that there were two distinct types of H_2O layers on the hydroxylated SiO_2 surface: a thin strongly adsorbed layer and a weakly adsorbed layer that was much thicker at high H_2O pressures. The strongly adsorbed layer had thicknesses ≤1.2 Å and was not lost by removing the H_2O pressure. The strongly adsorbed layer could be desorbed by heating the sample stage to 124 °C (397.15 K). The stability of the strongly adsorbed layer was consistent with an adsorption energy of >20 kcal/mol. In contrast, the weakly adsorbed layer could be added or removed by increasing or decreasing the H_2O pressure. The weakly adsorbed layer obtained much higher multilayer H_2O thicknesses at larger H_2O pressures. For example, the weakly adsorbed multilayer thickness was 7.5 Å at 92% relative humidity at 30.4 °C (32.5 Torr). Complementary in situ Fourier transform infrared (FTIR) studies were also performed on hydroxylated SiO_2 nanoparticles that were in qualitative agreement with the SE results.

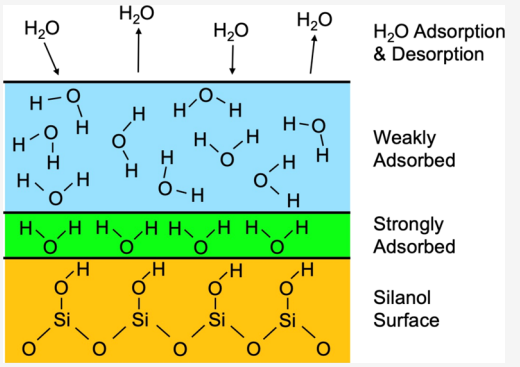

I. INTRODUCTION

The interaction between H_2O and SiO_2 surfaces is critical in the environment and in many technologies. H_2O on SiO_2 surfaces is important in the environment because SiO_2 is one of the most abundant oxides on earth and H_2O liquid and vapor are ubiquitous. H_2O on SiO_2 surfaces is vital in many technologies because SiO_2 is widely used as an insulator or optically transparent material. The interaction of H_2O at interfaces has been surveyed in a number of previous reviews.[1−5] For H_2O on SiO_2 surfaces, models have been developed for the SiO_2 surface defined by silanol (hydroxylated) or siloxane (dehydroxylated) groups.[6] Many experimental studies have also probed H_2O adsorption on SiO_2 surfaces.[7−10]

Although H_2O adsorption on hydroxylated SiO_2 surfaces has been studied extensively, there are still many questions about the H_2O adsorbed layer. For example, what is the exact H_2O coverage on the hydroxylated SiO_2 surface? What is the H_2O thickness in the initial vicinal or "ice-like"/ordered layer on hydroxylated SiO_2 surface? What is the H_2O thickness in the "liquid-like"/disordered layer in subsequent H_2O layers on the initial vicinal layer? How do these ice-like and liquid-like H_2O layer thicknesses depend on H_2O pressure and temperature? Answers to these questions will further expand our understanding of H_2O on hydroxylated SiO_2 surfaces.

The picture for "ice-like"/ordered and "liquid-like"/disordered H_2O on hydroxylated SiO_2 surfaces was developed from previous attenuated total reflection infrared (ATR-IR) spectroscopy studies.[7,11] By analyzing the O−H stretching vibrations, adsorbed H_2O on flat hydroxylated SiO_2 surfaces could be characterized as either ice-like/ordered or liquid-like/disordered. The ice-like water peak at 3230 cm^{-1} grows exclusively until a relative humidity (RH) of ∼30%.[7] Subsequently, the liquid-like peak at 3400 cm^{-1} grows along with the ice-like peak until a RH of ∼60%.[7] Further increases in RH are dominated by the liquid-like peak. The H_2O layer

Received: October 9, 2024
Revised: December 17, 2024
Accepted: December 18, 2024
Published: January 8, 2025

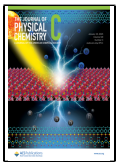

https://doi.org/10.1021/acs.jpcc.4c06859
J. Phys. Chem. C 2025, 129, 1666−1677

thicknesses were determined from the infrared absorbance of the H−O−H bending vibration. At 20.8 ± 0.5 °C, the ice-like layer has been reported to grow up to 3 monolayers (ML) or 8.5 Å where 1 ML = 2.82 Å at 30% RH.[7] An additional 1 ML or 2.82 Å to a thickness of 4 ML or 11.3 Å is added in a transitional ice-like/liquid-like H_2O layer between 30 and 60% RH.[7] The liquid-like layer has then been determined to grow up to 10 ML or 28.2 Å prior to reaching 100% RH.[7]

H_2O layer thicknesses on flat hydroxylated SiO_2 surfaces were also measured using X-ray photoelectron spectroscopy (XPS).[10] These XPS measurements were based on the electron mean free path through the water film. Isobaric experiments at 1.5, 3, and 4 Torr were employed where the temperature was varied to scan the RH.[10] The reported H_2O layer thicknesses were ∼2 ML or ∼6 Å at ∼15% RH and ∼4 ML or ∼13 Å at 75% RH.[10] These measured H_2O layer thicknesses were in approximate agreement with the previous infrared spectroscopy studies and other reported results.[7,11,12]

Ellipsometry analysis can also be utilized to measure the H_2O layer thickness on SiO_2 films on silicon wafers.[13] These measurements were recorded after washing the wafer with HF/HNO_3 followed by exposure to boiling HNO_3 for 5 min.[13] The measured H_2O layer thicknesses from these studies were less than the H_2O layer thickness from the previous infrared and XPS investigations. At 18 °C, the H_2O layer thickness was between 2−4 Å for RH values between 40−80%, respectively.[13] More recent ATR-IR measurements on flat hydrophilic SiO_2 surfaces also obtained smaller H_2O layer thicknesses between 6−8 Å at 20.8 ± 0.5 °C for RH values between 40−80%, respectively.[8] H_2O layer thicknesses on the hydrophobic Si−H surface were even lower at ∼1 Å for RH values between 40−80%, respectively.[8]

To quantify the thickness and nature of the H_2O layer on hydroxylated SiO_2 surfaces, in situ ellipsometry and Fourier transform infrared (FTIR) spectroscopy were utilized to study the H_2O layer on flat SiO_2 samples and SiO_2 nanoparticles, respectively. In situ ellipsometry allows for real-time monitoring of the H_2O layer thickness. In situ FTIR spectroscopy provides real-time identification of the species on the hydroxylated SiO_2 surface. These ellipsometric and FTIR spectroscopy measurements help clarify the H_2O layer thicknesses and nature of H_2O species on hydroxylated SiO_2 versus H_2O pressure at various substrate temperatures. These studies should be useful to understand the role of the H_2O layer on hydroxylated SiO_2 surfaces in various areas such as heterogeneous atmospheric chemistry[12] and tribology.[14]

Adsorbed H_2O layers on thin-film surfaces may also be employed for etching by a liquid layer in a vacuum environment. Many etching processes are conducted in wet aqueous solutions.[15] Etching in an adsorbed H_2O layer may extend wet etching to liquid-like etching in vacuum. For example, adsorbed H_2O layers may dissolve various etchants such as hydrogen fluoride (HF). SiO_2 could be etched under vacuum by HF in a liquid H_2O layer during HF and H_2O codosing.[16]

II. EXPERIMENTAL SECTION

II.I. Vacuum Chamber and Substrates. The H_2O adsorption experiments on flat SiO_2 samples were performed in a warm-wall V-shaped vacuum chamber with a cooled sample stage as illustrated in Figure S1, Supporting Information. This chamber incorporated a V-shaped tube to enable in situ spectroscopic ellipsometry (iSE) at an angle of incidence of 70°. Static dose conditions were possible using a pneumatic poppet valve at the exhaust port of the chamber. The chamber walls were heated with a custom ceramic heater (Valin Corporation). The chamber was pumped with a dual-stage mechanical pump (Pascal 2010 C1, Pfeiffer Vacuum). The base pressure of the chamber was 20 mTorr. The pressure was monitored with a capacitance manometer (MKS Instruments, Inc.)

The distinguishing feature of the chamber was the design for the cooled sample stage shown in Figure 1. In this design, a

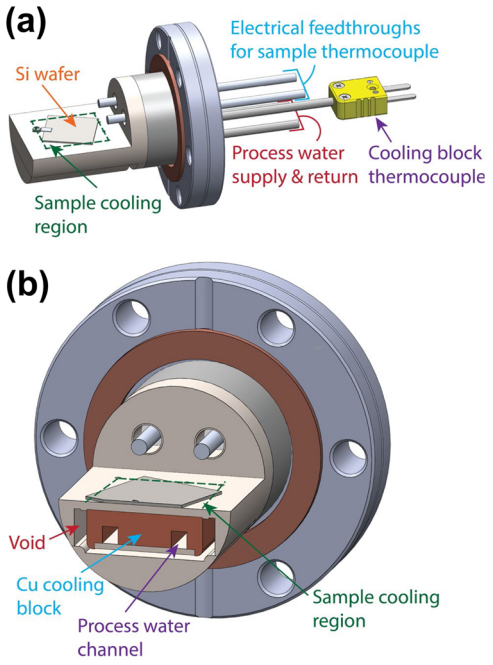

Figure 1. (a) Cooled sample stage showing the horizontal sample stage inside the chamber and electrical feedthroughs and coolant lines outside the chamber. (b) Cross sectional view of horizontal sample stage with sample cooling region defined by Cu cooling block.

cylinder that extended into the vacuum chamber was brazed to a Conflat flange. A hemicylinder was then attached at the end of the cylinder as illustrated in Figure 1a. The rectangular top of this hemicylinder was the horizontal sample stage. The interior of the cylinder and hemicylinder was open to atmosphere and permitted access for the water coolant supply and return lines and a K-type thermocouple probe.

A copper cooling block was fixtured underneath the rectangular top of the hemicylinder as shown in Figure 1b. The sample stage was cooled by passing water coolant though the copper block with a recirculating chiller (Thermo Scientific Accel 500 LT). The coolant temperature was maintained by the chiller. There was a void space between the copper block and the hemicylinder except where the copper block attached to the bottom of the rectangular top of the hemicylinder. This design defined the sample cooling region and ensured that the sample was at the coldest temperature in the chamber. Otherwise, H_2O condensation on other colder surfaces becomes a serious problem at high relative humidity (RH).[17]

SiO_2 films on silicon wafer samples (Silicon Valley Microelectronics, Inc.) were used for the water adsorption experiments. These flat samples had a SiO_2 thickness of 500 nm formed by wet thermal oxidation of the silicon wafer. Individual coupons cut from these wafers were 3 cm × 2 cm.

https://doi.org/10.1021/acs.jpcc.4c06859
J. Phys. Chem. C 2025, 129, 1666−1677

The samples were cleaned by turning off the coolant and removing the liquid from the sample stage to allow the warm reactor walls to heat the samples. A chamber temperature of 145 °C was able to heat the sample stage to 124 °C. The samples were heated at 124/145 °C stage/chamber temperatures for ≥1 h. After heating to 124 °C, the sample was exposed to a H_2O_2 plasma for ∼30 s. The plasma was achieved by flowing ∼100 mTorr of H_2O_2 into the chamber while discharging a Tesla coil through the gas in the chamber. The H_2O_2 plasma was stopped after the ellipsometric Delta signal became constant indicating removal of ambient contaminations.

In addition to cleaning carbonaceous debris from the coupons, the H_2O_2 plasma also rehydroxylated the SiO_2 surface and produced a hydrophilic surface.[18] Water contact angle measurements taken prior to cleaning showed a contact angle of 51 ± 1°. Water contact angles after cleaning were <5°. After precleaning and hydroxylation of the SiO_2 surfaces, the samples were cooled down to the experimental temperatures. Liquid H_2O (HPLC grade, Fisher Chemical) was housed in a stainless-steel cylinder and heated to 90 °C to provide sufficient H_2O vapor pressure. Before the experiments and in between H_2O exposures, the chamber was purged with ultrahigh-purity-grade (UHP) argon (Ar) gas (99.999%, Airgas).

II.II. Spectroscopic Ellipsometry. A spectroscopic ellipsometer (iSE, J.A. Woollam) at an incident angle of 70° was used to monitor the H_2O layer thickness on the SiO_2 surface in situ and in real time. The wavelength range for the ellipsometric measurements was 400−1000 nm. The ellipsometer continuously recorded measurements during H_2O exposures, averaging each data point for 5 s. CompleteEASE software version 6.57 (J.A. Woollam Co.) was used to model the ellipsometric data.

The ellipsometer model included the top H_2O layer, the SiO_2 film and the underlying silicon support. The modeling of the H_2O layer assumed a refractive index of n = 1.337.[19] This refractive index is in good agreement with other literature reports for liquid water.[20,21] The refractive index for ambient H_2O vapor can be neglected in the ellipsometer model.[22] The 500 nm SiO_2|Si samples were modeled as a layer stack of the SiO_2_JAW[23]| 10 Å INTR_JAW[23]| Si Temp JAW[24,25] material files from the CompleteEASE library.

The noise in the H_2O layer thickness was ±0.03 Å. This value for the precision of the ellipsometry measurements was derived from 30 repeated SE measurements at stabilized temperature and Ar purge conditions.[26] This high precision was obtained using an interference enhancement effect from the 500 nm SiO_2|Si sample.[27] This SE sensitivity is approximately 2 orders of magnitude below the 2.82 Å diameter of an H_2O molecule. Measured H_2O thicknesses less than 2.82 Å represent an average H_2O coverage. This average H_2O coverage is integrated over the SE beam area of ∼0.5 × 1 cm^2. H_2O thicknesses <2.82 Å indicate an incomplete H_2O monolayer. Based on the number density of ice, one monolayer of H_2O has a coverage of ∼1.0×10^{15} H_2O molecules/cm^2.[28]

II.III. Calibrated Temperature Measurements. Temperature calibration is important to know the saturation H_2O vapor pressure corresponding to the sample temperature. As shown in Figure 1, the sample stage was designed to ensure that the sample cooling region was at the coldest temperature in the chamber.[17] A thermocouple was located in the copper block underneath the cooled sample stage. Even with this design, preliminary experiments revealed that the sample temperature was between the temperature of the cooled stage and the chamber. To minimize the difference between the sample and stage temperatures, an indium foil was sandwiched between the sample and the stage to improve the thermal conductivity.

The temperature of the cooled stage was calibrated by increasing the H_2O pressure. Using a constant H_2O flow into the chamber with no vacuum pumping, the H_2O pressure increased linearly with time. When the H_2O pressure reached the saturation pressure of the cooled stage, H_2O condensed on the stage and changed the slope of the H_2O pressure versus time. This saturation vapor pressure was equated to 100% relative humidity (RH). The saturation vapor pressure was then used to calculate the temperature of the sample stage based on known saturation vapor pressures for H_2O at different temperatures.

The saturation pressures for H_2O at the different stage temperatures were then compared with saturation pressures derived from spectroscopic ellipsometry measurements of the H_2O layer thickness on the sample. These saturation pressures were identified by the threshold H_2O pressures that led to an overshoot in the H_2O layer thickness on the sample. These threshold H_2O pressures were also used to determine the sample temperature. The temperatures determined by these two measurements of the saturation pressure were in good agreement.

II.IV. FTIR Chamber and Substrates. In situ transmission FTIR measurements of H_2O adsorption on SiO_2 nanoparticles were performed in a chamber equipped with an FTIR spectrometer and two BaF_2 optical windows.[29] The FTIR spectrometer (Nicolet 6700 FTIR from Thermo Scientific) utilized a high-sensitivity liquid-N_2-cooled mercury cadmium telluride (MCT-B) detector. The spectrometer, mirror, and detector were purged with dry, CO_2-free air. A total of 40 scans at 4 cm^{-1} resolution from 400 to 4000 cm^{-1} were recorded for each collected spectrum. The BaF_2 windows were obtained from Crystran (Part number BAFP38−3) and were mounted to the chamber on window flanges. These flanges were heated to 50 °C to reduce H_2O adsorption on the window surfaces.

The transmission FTIR measurements were performed on high surface area SiO_2 nanoparticles (98%, US Research Nanomaterials Inc.) with an average diameter of 60−70 nm. The high surface area of these particles improved the signal-to-noise ratio of the FTIR measurements compared with a flat sample.[30,31] Sample preparation involved pressing the SiO_2 nanoparticles into a tungsten grid support (Tech-Etch). The tungsten grids were 2 × 3 cm^2. Each grid was 50 μm thick with 100 grid lines per inch. The amount of SiO_2 nanoparticles in the grid varied for different samples. This variability led to different infrared absorption for the bulk SiO_2 absorption at 900−1300 cm^{-1}.

The SiO_2 nanoparticles were loaded into the chamber and the chamber was evacuated to a base pressure of ∼30 mTorr. The entire chamber, BaF_2 windows, and sample were then heated to 250 °C and exposed to a continuous viscous O_3 flow at 0.35 Torr for 1 h. This O_3 exposure removed the residual adventitious carbon and defined the initial hydroxylated SiO_2 nanoparticles. The O_3 was produced by a TMEiC O_3 generator (Model OG-6OH) operating at an input O_2 flow of 0.5 L/min and an output O_3 concentration of 200 g/m^3 or approximately 13 wt % O_2/87 wt % O_3. This O_3 treatment combined with heating the BaF_2 window flanges also ensured that negligible

https://doi.org/10.1021/acs.jpcc.4c06859
J. Phys. Chem. C 2025, 129, 1666−1677

H_2O adsorption occurred on the BaF_2 window surfaces at H_2O pressures ≤10 Torr.

III. RESULTS AND DISCUSSION

III.I. Temperature and Surface Characterization. Temperature calibration was obtained by increasing the H_2O pressure using a constant H_2O flow into the chamber with no pumping. The H_2O pressure increases linearly until the H_2O begins to condense on the sample stage. At this point, the H_2O pressure versus time displays a reduced slope corresponding to H_2O condensation.

Examples of these H_2O pressure versus time curves are shown in Figure S2, Supporting Information. 100% relative humidity was identified by the bends in the pressure versus time curves. 100% relative humidities were found to be 32.5 Torr corresponding to a stage temperature of 30.4 °C; 27.0 Torr corresponding to a stage temperature of 27.2 °C; and 15.6 Torr corresponding to a stage temperature of 18.1 °C.

Surface preparation affects the chemical properties of the SiO_2 surface.[11] To demonstrate how the surface hydrophilicity depends on surface preparation, water contact angles were measured for three differently prepared SiO_2 samples. The samples examined were: (1) a sample with no surface cleaning; (2) a sample that was heated at 124/145 °C stage/chamber temperatures for 2 h; and (3) a sample that was heated at 124/145 °C stage/chamber temperatures for 2 h and then cleaned using a 50 wt % H_2O_2 plasma for 30 s.

Subsequently, water contact angles were measured for the SiO_2 surfaces prepared using these three methods. In these measurements, three water droplets were placed on each surface and a side-view was imaged as shown in Figure S3, Supporting Information. A water droplet on a very hydrophobic surface will remain "dome shaped" as the water droplet is more repelled from the SiO_2 surface. A water droplet on a hydrophilic surface will appear to be flat resulting from strong attractive interactions. The sample with no surface cleaning had the highest water contact angle of 51 ± 1°. The sample that was only heated was slightly more hydrophilic with a water contact angle of 38 ± 1°. Lastly, the sample that was heated and cleaned with H_2O_2 plasma was the most hydrophilic with a water contact angle of <5°.

III.II. H_2O Layer Thickness with and without H_2O Vapor Pressure. *III.II.I. Spectroscopic Ellipsometry Measurements.* H_2O layer thicknesses were measured using spectroscopic ellipsometry after different preparations of the SiO_2 surface. For these experiments, water vapor was dosed statically into the chamber and then purged from the chamber with Ar gas. This dose-then-purge procedure was repeated 10 times. For the results shown in Figure 2, the H_2O vapor was increased to 20 Torr and held statically for 30 min prior to an Ar purge for 10 min. Figure 2a shows the results for a SiO_2 sample at 30.4 °C that was previously heated at stage/chamber temperatures of 125/145 °C and cleaned with H_2O_2 plasma. Figure 2b displays the results for a SiO_2 sample at 30.4 °C that was only heated at stage/chamber temperatures of 125/145 °C.

Initially, there was no H_2O layer thickness on either SiO_2 sample at 30.4 °C in Figure 2a,b. During H_2O exposures at 20 Torr, Figure 2a reveals that the SiO_2 sample that was heated and cleaned with H_2O_2 plasma adsorbed a much thicker H_2O layer compared with the SiO_2 surface that was only heated as shown in Figure 2b. The sample that was heated and cleaned with H_2O_2 plasma in Figure 2a had a H_2O thickness of ~2.2 Å during the first 20 Torr exposure and ~3.3 Å during the second 20 Torr exposure. In contrast, the sample that was only heated in Figure 2b had a H_2O thickness of ~0.2 Å during the first 20 Torr exposure and ~0.5 Å during the second 20 Torr exposure. The H_2O thicknesses only slightly increase versus H_2O exposure after the second H_2O exposure in both Figure 2a,b.

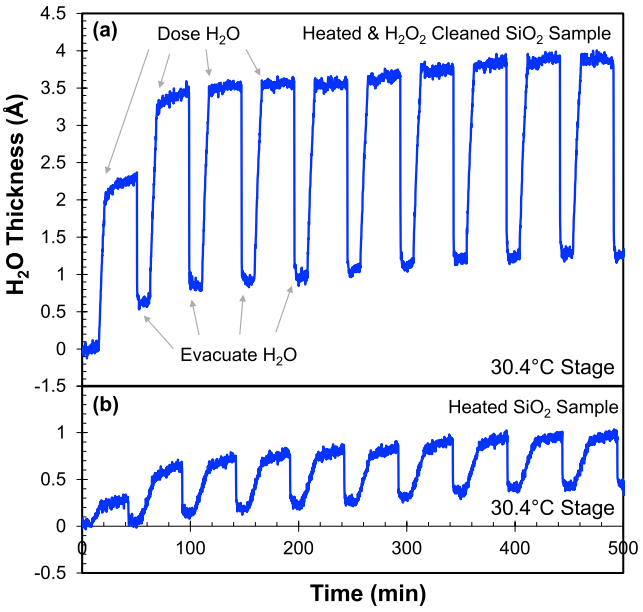

Figure 2. H_2O thicknesses on SiO_2 samples during 10 static H_2O exposures at 20 Torr for 30 min at a stage temperature of 30.4 °C. There was a 10 min Ar purge between each H_2O exposure. This procedure was conducted on (a) hydroxylated sample from heating to stage/chamber temperatures of 124/145 °C for 1 h and then cleaning with H_2O_2 plasma for 30 s and (b) sample from heating to stage/chamber temperatures of 124 °C/145 °C for 1 h.

After removal of the H_2O exposure at 20 Torr, Figure 2a shows that the H_2O thickness quickly drops to a much lower value. This H_2O thickness reduction is consistent with the desorption of a large fraction of the H_2O coverage. At 30.4 °C, the H_2O pressure of 20 Torr can maintain a steady-state H_2O coverage on the hydroxylated SiO_2 surface. In the absence of the H_2O pressure, the majority of the H_2O coverage desorbs from the surface. This behavior indicates that the H_2O coverage is dynamic.[32,33] The H_2O coverage is defined by the competing adsorption and desorption rates for H_2O on hydroxylated SiO_2 at 20 Torr and 30.4 °C. The H_2O coverage that is easily desorbed after removing the H_2O pressure is defined as "weakly adsorbed" H_2O.

In addition, Figure 2a shows that a portion of the H_2O thickness remained after the H_2O pressure of 20 Torr was removed from the chamber. This residual H_2O thickness was larger for the sample that was heated and cleaned with H_2O_2 plasma compared with the sample that was only heated as shown in Figure 2b. For the SiO_2 sample in Figure 2a, the residual H_2O thickness was ~0.6 Å after the first 20 Torr exposure and ~0.8 Å after the second 20 Torr exposure. For the SiO_2 sample in Figure 2b, the residual H_2O thickness was <0.1 Å after the first 20 Torr exposure and ~0.2 Å after the second 20 Torr exposure. In addition, the residual H_2O thicknesses slightly increased versus H_2O exposure after the second H_2O exposure in both Figure 2a,b. The residual H_2O coverage that is retained on the hydroxylated SiO_2 surface after

https://doi.org/10.1021/acs.jpcc.4c06859
J. Phys. Chem. C 2025, 129, 1666−1677

removing the H_2O pressure is defined as "strongly adsorbed" H_2O.

III.II.II. FTIR Measurements. The presence of residual H_2O on the SiO_2 surface after H_2O exposures was also confirmed by FTIR measurements on SiO_2 nanoparticles at 25 °C. Figure 3a shows the absorbance results at 25 °C for the initial hydroxylated SiO_2 nanoparticles, the hydroxylated SiO_2 nanoparticles exposed to a H_2O pressure of 1 Torr for 1 min, and then after evacuation for 1 min. For a H_2O pressure of 1 Torr/1 min, the FTIR spectrum was recorded in the first 15 s after the H_2O exposure of 1 Torr/1 min while the H_2O pressure of 1 Torr was still present. The absorbance from gas phase H_2O has been subtracted from the spectra in Figure 3a using the absorbance spectrum for gas phase H_2O with the SiO_2 nanoparticles removed from the infrared beam path.

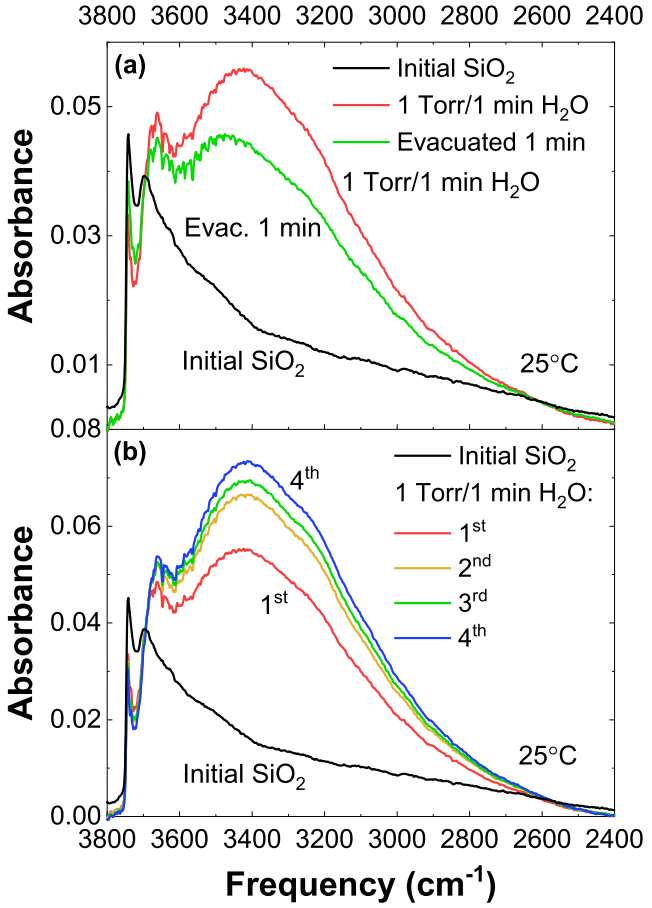

Figure 3. (a) IR absorbance spectra of initial SiO_2 particle sample prior to H_2O exposure, in the first 15 s after an H_2O exposure of 1 Torr/1 min while the H_2O pressure of 1 Torr was still present, and after evacuation for 1 min following 1 Torr/1 min H_2O exposure. (b) IR spectra of initial SiO_2 particle sample prior to H_2O exposure, and then during four subsequent 1 Torr/1 min H_2O vapor exposures where the IR spectra were recorded in the first 15 s after the 1 Torr/1 min H_2O exposures while the H_2O pressures of 1 Torr were still present. Absorbance from gas phase H_2O has been removed from the spectra in panel (a, b).

For the spectrum for the initial hydroxylated SiO_2 nanoparticles, the isolated SiO−H stretching vibration is observed at 3740 cm^{-1}. The peak in the broad distribution of hydrogen-bonded SiO−H stretching vibrations is monitored at 3690 cm^{-1}. For the spectrum recorded in the first 15 s after the 1 Torr/1 min H_2O exposure during the H_2O exposure at 1 Torr, the absorbance from O−H stretching vibrations from adsorbed H_2O increases substantially between 2600−3700 cm^{-1}. The gas phase H_2O absorbance observed at frequencies from 3400−4000 cm^{-1} have been removed from the spectrum.[34] After evacuation for 1 min, a large fraction of the absorbance from adsorbed H_2O is still present. Similar to the results shown in Figure 2, the retention of this absorbance indicates that residual H_2O is present on the SiO_2 surface at 25 °C after H_2O exposure followed by H_2O evacuation.

The adsorbed H_2O features on the SiO_2 nanoparticles also grow in intensity with successive H_2O exposures. The FTIR measurements displayed in Figure 3b show the infrared absorbance after repeated H_2O exposures for 1 Torr/1 min followed by H_2O evacuation. The FTIR spectra were recorded in the first 15 s after the H_2O pressure of 1 Torr/1 min while the H_2O pressure of 1 Torr was still present. The absorbance from gas phase H_2O has again been subtracted from the spectra in Figure 3b. There is then an evacuation time of 1 min prior to the next H_2O pressure of 1 Torr/1 min. Figure 3b shows that the infrared absorbance is approaching a saturation value by the third and fourth H_2O exposure for 1 Torr/1 min. These results are similar to the results for the H_2O layer thickness measured by spectroscopic ellipsometry in Figure 2a. There is a H_2O layer adsorbed on the SiO_2 surface during the H_2O exposures. This adsorbed H_2O layer grows slowly with progressive H_2O exposures.

III.III. Dependence of H_2O Layer Thickness on Increasing H_2O Pressure. *III.III.I. Spectroscopic Ellipsometry Measurements.* The effect of H_2O pressure on the H_2O thickness was examined on hydroxylated SiO_2 surfaces that had been cleaned using the heating and H_2O_2 plasma treatment. The H_2O exposures were initially conducted at a stage temperature of 30.4 °C. The H_2O pressure was increased to the target pressure and then left in the static chamber to evolve with time for 30 min. Subsequently, the chamber was purged with inert Ar gas for 10 min before starting a new H_2O exposure. The water exposures were conducted in order of increasing pressures from 2 to 32.5 Torr.

Figure 4a shows the thickness of the H_2O layer monitored by in situ ellipsometry at the various H_2O pressures. The H_2O thickness increases at higher H_2O pressures. The H_2O thicknesses range from ~0.5 Å at 5 Torr to ~7 Å at 27.5 Torr. At H_2O pressures greater than 27.5 Torr, the H_2O thickness starts higher and then reduces to a lower thickness versus time. This behavior is related to the H_2O pressure reaching the saturation vapor pressure for the stage temperature of 30.4 °C. The saturation vapor pressure was determined to be 32.5 Torr for the stage temperature of 30.4 °C based on the calibrations shown in Figure S2, Supporting Information. The H_2O pressure approaches and exceeds the saturation vapor pressure at H_2O pressures of 30 and 32.5 Torr, respectively.

Figure 4b displays the measured H_2O pressures in the chamber. Up to H_2O pressures of 27.5 Torr, the H_2O pressures have fairly flat tops. For H_2O pressures of 30 and 32.5 Torr, the H_2O pressure overshoots and then decreases versus time. This reduction is related to H_2O condensing because the initial H_2O pressure is close to or higher than the saturation H_2O pressure. This decrease corresponds with H_2O thicknesses in Figure 4a that also overshoot and then return to a lower H_2O thickness.

https://doi.org/10.1021/acs.jpcc.4c06859
J. Phys. Chem. C 2025, 129, 1666−1677

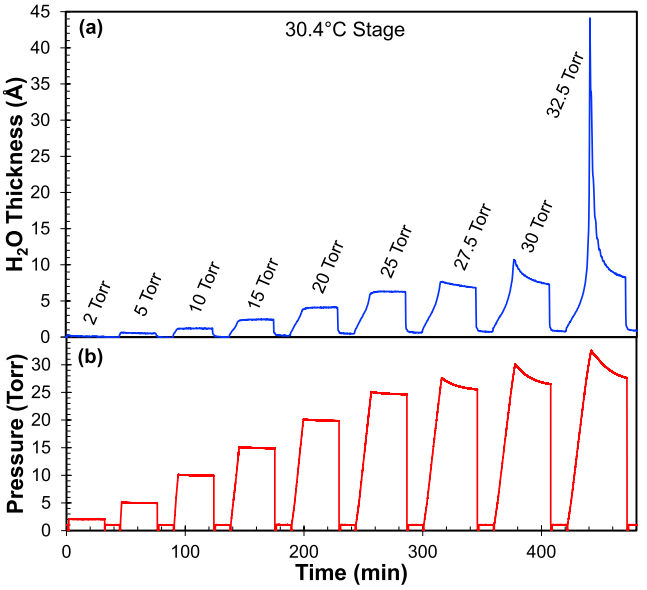

Figure 4. (a) H_2O layer thickness on hydroxylated SiO_2 sample at stage temperature of 30.4 °C for progressively increasing H_2O pressures during 30 min static H_2O exposures. There was a 10 min Ar purge in between each H_2O exposure. (b) Pressures in chamber during H_2O exposures in panel (a).

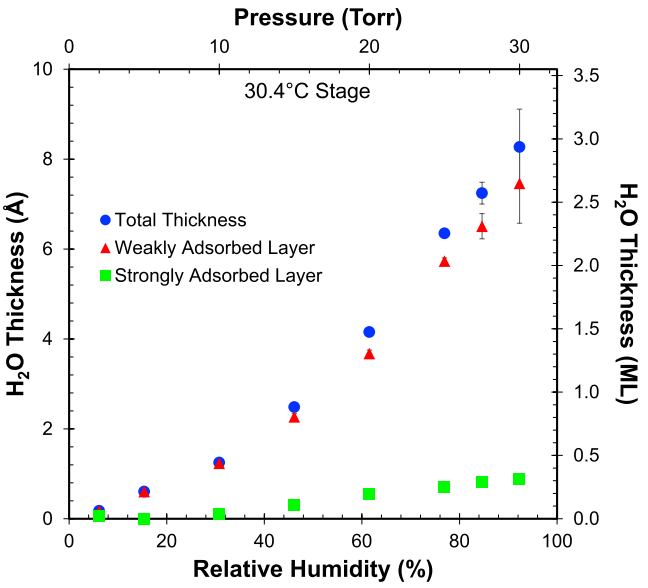

Figure 5. Thickness of total H_2O layer, weakly adsorbed H_2O layer, and strongly adsorbed H_2O layer on SiO_2 sample at a stage temperature of 30.4 °C corresponding to various H_2O pressures shown in Figure 4.

The H_2O thicknesses in Figure 4a also reveal that there is a residual H_2O thickness remaining on the hydroxylated SiO_2 surface after the various H_2O exposures at different H_2O pressures. This residual H_2O thickness is not removed by the 10 min Ar purge after the H_2O exposure. In addition, this residual H_2O thickness increases slowly with the H_2O exposures at progressively higher H_2O pressures. The residual H_2O thickness is <0.1 Å after the 5 Torr H_2O exposure. The residual H_2O thickness increases to ~0.7 Å after the 27.5 Torr H_2O exposures.

III.III.II. Thicknesses for Strongly and Weakly Adsorbed H_2O Layers versus H_2O Pressure. The total H_2O thickness at a given H_2O pressure can be characterized by (1) the thickness of the strongly adsorbed residual H_2O layer that remains after the H_2O exposure and (2) the thickness of the more weakly adsorbed H_2O layer on top of the strongly adsorbed layer. Figure 5 shows these H_2O thicknesses corresponding to the results in Figure 4. The H_2O thickness in Angstroms is converted to a H_2O thickness in monolayers (ML) based on a conversion factor of 1 ML = 2.82 Å.[2,7,8] The mean van der Waals diameter of H_2O is 2.82 Å.[7,8] This conversion factor of 1 ML = 2.82 Å is slightly larger than 1 ML = 2.76 Å for hexagonal ice (ice I).[28,35]

The total H_2O thickness versus pressure in Figure 5 is somewhat similar to the general shape of multilayer adsorption curves expected from the Brunauer–Emmett–Teller (BET) model.[36] The total H_2O thickness increases steadily versus pressure. The strongly adsorbed layer levels off at a H_2O thickness of ~0.9 Å. The weakly adsorbed H_2O layer thickness also increases steadily with H_2O pressure to ~6.5 Å at 27.5 Torr. The weakly adsorbed H_2O layer thickness increases to ~7.5 Å at 30 Torr which is near 100% relative humidity at 30.4 °C.

The absolute total H_2O thickness versus pressure in Figure 5 is comparable to ATR-IR results for water on hydrophilic SiO_2 surfaces.[8] The absolute total H_2O thickness results in Figure 5 are also close to the ellipsometry results for water on silicon wafers at 18 °C after washing the wafer with HF/HNO_3 followed by exposure to boiling HNO_3 for 5 min.[13] In contrast, the absolute total H_2O thickness versus pressure in Figure 5 is about 2 times less than earlier ATR-IR and XPS results for the water thickness on hydrophilic surfaces at 20.8 ± 0.5 °C.[7,10,11]

The strongly and weakly adsorbed H_2O thicknesses can also be compared with the ice-like/ordered and liquid-like/disordered layers identified in the ATR-IR studies.[8] Relative to the total thickness, the thickness of the ice-like/ordered layer in the ATR-IR studies is larger than the strongly adsorbed layer in Figure 5. In addition, relative to the total thickness, the thickness of the liquid-like layer in the ATR-IR studies is less than the weakly adsorbed layer in Figure 5.

In addition to this research on flat hydroxylated SiO_2 surfaces and the above-mentioned investigations on flat hydroxylated SiO_2 surfaces, there have also been investigations on H_2O adsorption on hydroxylated SiO_2 particles.[3] Many techniques have been utilized to measure the H_2O surface coverage versus H_2O relative humidity.[37−40] These studies yield a functional form for the multilayer adsorption that is similar to the results in Figure 5 for the total H_2O layer thickness. However, the absolute H_2O coverages at 90% RH from these different techniques vary from about 2−7 ML.[3]

III.III.III. FTIR Measurements. Complementary FTIR spectra were also recorded for H_2O adsorption on SiO_2 nanoparticles. H_2O was exposed to initial hydroxylated SiO_2 nanoparticles at 25 °C at varying pressures between 0.5−5 Torr for 1 min. The FTIR spectra were recorded in the first 15 s after the H_2O pressure at the given H_2O pressure for 1 min while the H_2O pressure was still present. After the H_2O exposure, the chamber was evacuated for 5 min. These FTIR experiments mirror the ellipsometry experiments shown in Figure 4a where the increasing H_2O pressures are separated by purge times.

Figure 6 shows the infrared absorbance for the O−H stretching vibrations from 3000 to 3800 cm^{-1}. This range covers the O−H stretching vibrations from adsorbed H_2O and the SiOH surface species on the hydroxylated SiO_2 surface.

https://doi.org/10.1021/acs.jpcc.4c06859
J. Phys. Chem. C 2025, 129, 1666−1677

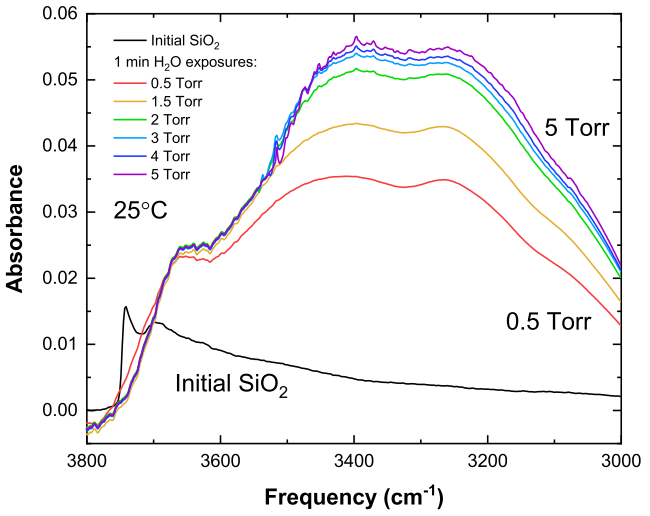

Figure 6. IR absorbance spectra at 25 °C from initial SiO_2 particles and then during various H_2O exposures for 1 min at various increasing H_2O pressures. IR spectra were recorded in the first 15 s after the 1 min H_2O exposures while the H_2O pressures were still present. Absorbance from gas phase H_2O has been subtracted from the spectra.

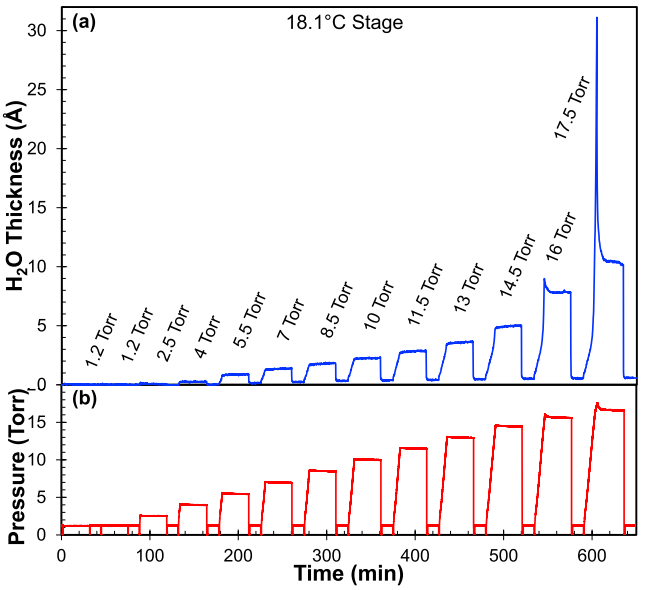

Figure 7. (a) H_2O layer thickness on hydroxylated SiO_2 sample at stage temperature of 18.1 °C for progressively increasing H_2O pressures during 30 min static H_2O exposures. There was a 10 min Ar purge in between each H_2O exposure. (b) Pressure in chamber during H_2O exposures in panel (a).

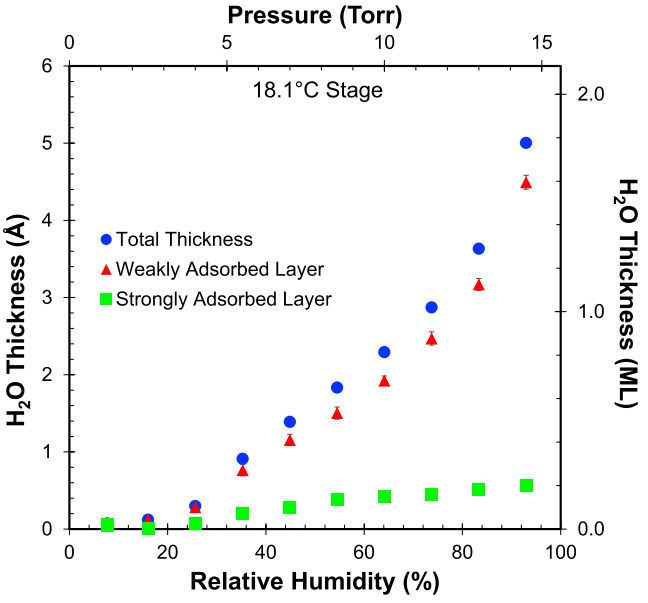

Figure 8. Thickness of total H_2O layer, weakly adsorbed H_2O layer, and strongly adsorbed H_2O layer on SiO_2 sample at a stage temperature of 18.1 °C corresponding to various H_2O pressures shown in Figure 7.

The absorbance from gas phase H_2O has been removed from the spectra in Figure 6. The results are similar to the ellipsometry results that observed larger H_2O thicknesses at higher H_2O pressures in Figure 4a. The FTIR results in Figure 6 indicate that the absorbance increases progressively at higher H_2O pressure.

III.IV. Dependence of H_2O Layer Thickness on Substrate Temperature. Experiments were also performed at lower stage temperatures of 18.1 and 27.2 °C. These experiments were similar to the experiments shown in Figure 4 at the stage temperature of 30.4 °C. However, the H_2O pressures were lower because of the lower saturation H_2O vapor pressures. The saturation H_2O vapor pressures at 18.1 and 27.2 °C are 15.6 and 27.0 Torr, respectively. These saturation vapor pressures were determined based on the calibrations shown in Figure S2, Supporting Information.

Figure 7a shows the H_2O thicknesses for increasing H_2O pressures at the stage temperature of 18.1 °C. Like the results shown in Figure 4a, the H_2O exposures were conducted for 30 min. Ar purged the chamber for 10 min between the water exposures. The H_2O thicknesses increase at higher H_2O pressures. The H_2O thicknesses range from ~0.9 Å at 5.5 Torr to ~5.0 Å at 14.5 Torr. The H_2O thicknesses in Figure 7a also show that there is residual H_2O thickness remaining after the various H_2O exposures. This residual H_2O thickness is not removed by the Ar purge after the H_2O exposure. This residual H_2O thickness increases slowly with the H_2O exposures to progressively higher H_2O pressures. For example, the residual H_2O thickness is ~0.2 Å after the 5.5 Torr H_2O exposure. The residual H_2O thickness increases to ~0.5 Å after the 14.5 Torr H_2O exposures.

At H_2O pressures greater than 14.5 Torr, the H_2O thickness overshoots and then returns to a lower thickness. This behavior is caused by the H_2O pressure exceeding the saturation vapor pressure for the stage temperature of 18.1 °C. At H_2O pressures of 16 and 17.5 Torr, the H_2O pressure initially exceeds the saturation vapor pressure. Figure 7b displays the measured H_2O pressures in the chamber. Up to a H_2O pressure of 14.5 Torr, the H_2O pressures are very constant versus time. For the higher H_2O pressures of 16 and 17.5 Torr, the H_2O pressure has a small transient to higher pressure prior to a short reduction versus time. These H_2O pressure transients correspond with the H_2O thicknesses that increase and then return to a lower H_2O thickness.

Figure 8 shows the strongly adsorbed residual H_2O thicknesses and the weakly adsorbed H_2O thicknesses for the various H_2O pressures corresponding to the results in Figure 7 at 18.1 °C. The results are consistent with multilayer adsorption at higher H_2O pressure. The strongly adsorbed

https://doi.org/10.1021/acs.jpcc.4c06859
J. Phys. Chem. C 2025, 129, 1666−1677

layer levels off at a H_2O thickness of 0.5 Å at 18.1 °C. The weakly adsorbed H_2O layer thickness increases steadily with H_2O pressure and increases more rapidly as the RH approaches 100%.

Figure 9 shows the H_2O thicknesses for a range of H_2O pressures at the stage temperature of 27.2 °C. These

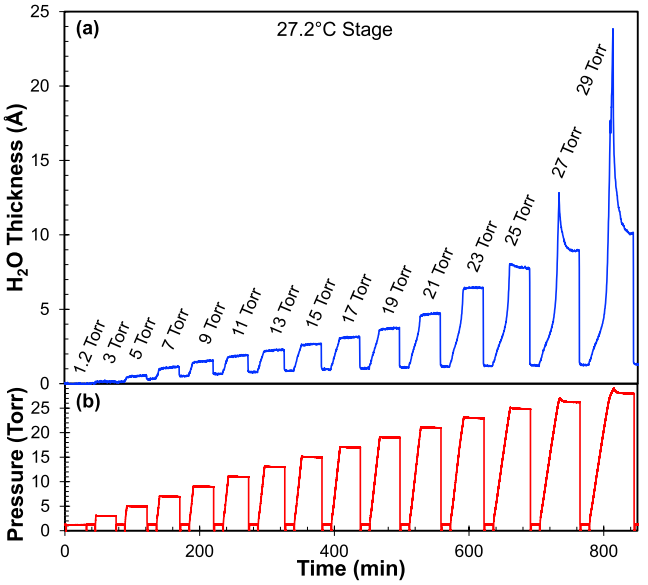

Figure 9. H_2O layer thickness on hydroxylated SiO_2 sample at stage temperature of 27.2 °C for progressively increasing H_2O pressures during 30 min static H_2O exposures. There was a 10 min Ar purge in between each H_2O exposure. (b) Pressure in chamber during H_2O exposures in panel (a).

experiments were also performed like the experiments shown in Figures 4 and 7. The H_2O thicknesses increase at higher H_2O pressures. The H_2O thicknesses range from ~0.5 Å at 5 Torr to ~7.8 Å at 25 Torr. The H_2O thicknesses in Figure 9a also show that there is a residual H_2O thickness remaining after the various H_2O exposures. This residual H_2O thickness increases slowly with the H_2O exposures to progressively higher H_2O pressures. The residual H_2O thickness is ~0.3 Å after the 5 Torr H_2O exposure. The residual H_2O thickness increases to ~1.2 Å after the 25 Torr H_2O exposures.

At H_2O pressures greater than 25 Torr, the H_2O thickness overshoots and then returns to a lower thickness. This behavior is again related to the H_2O pressure exceeding the saturation vapor pressure for the stage temperature of 27.2 °C. Figure 9b displays the measured H_2O pressures in the chamber. Up to a H_2O pressure of 25 Torr, the H_2O pressures are constant versus time. For H_2O pressures of 27 and 29 Torr, the H_2O pressure increases to a higher pressure before returning to a lower pressure. These H_2O pressure transients correspond with the H_2O thicknesses that overshoot and then return to a lower H_2O thickness.

Figure 10 shows the strongly adsorbed residual H_2O thicknesses and the weakly adsorbed H_2O thicknesses for the various H_2O pressures at 27.2 °C corresponding to the results in Figure 9. Like the results in Figures 5 and 8, Figure 10 is consistent with multilayer adsorption. The strongly adsorbed layer levels off at a H_2O thickness of ~1.2 Å at 27.2 °C. The weakly adsorbed H_2O increases steadily with H_2O pressure and increases more rapidly as the RH approaches 100%.

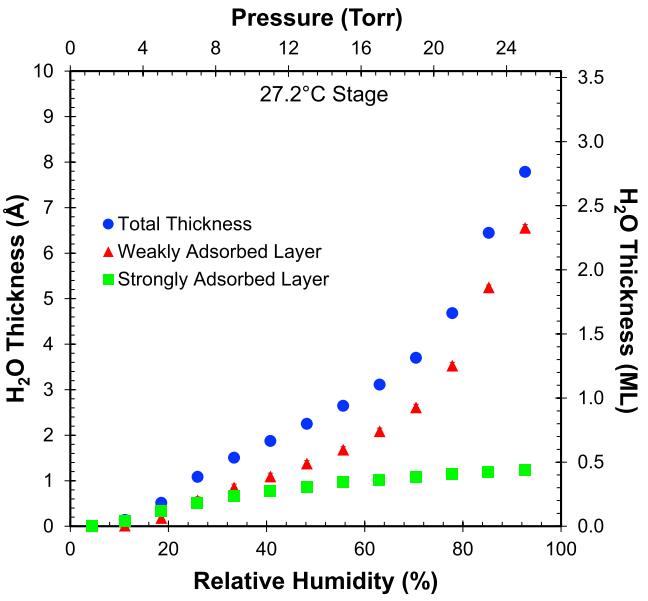

Figure 10. Thickness of total H_2O layer, weakly adsorbed H_2O layer, and strongly adsorbed H_2O layer on SiO_2 sample at a stage temperature of 27.2 °C corresponding to various H_2O pressures shown in Figure 9.

Although Figures 5, 8 and 10 show plots of H_2O thickness versus RH that are consistent with multilayer adsorption, they are not fit well using the simple BET model.[36] Reliable c values from the BET model could not be determined that would establish the energy difference between the H_2O adsorbates in the first layer on the hydroxylated surface and the subsequent H_2O molecules in the H_2O multilayer. Consequently, the adsorption energies for H_2O were determined using other methods as discussed below.

III.V. Adsorption Energies for Strongly and Weakly Adsorbed H_2O on Hydroxylated SiO_2. The adsorption energy for H_2O in the strongly adsorbed residual layer that remains on the hydroxylated SiO_2 surface after the H_2O exposure can be estimated using the Redhead equations for thermal desorption.[41] The equation for first-order desorption from the Redhead treatment is[41]

$$N(t) = -\mathrm{d}\Theta/\mathrm{d}t = \nu_1 \Theta \exp[-E/RT] \quad (1)$$

In this equation, $N(t)$ is the desorption signal, $d\Theta/dt$ is the time derivative of the coverage, ν_1 is the desorption preexponential, E is the desorption activation energy, and T is the temperature. The desorption activation energy is assumed to be equal to the adsorption energy.

Stable H_2O coverage on the hydroxylated SiO_2 surface can be equated to a low desorption rate and a long H_2O residence time. For example, stability of the strongly adsorbed residual layer at 25 °C is consistent with a desorption peak temperature T_p > 25 °C during a linear temperature ramp. Based on a desorption peak temperature T_p > 25 °C and assuming a desorption preexponential of $\nu_1 = 1 \times 10^{13}$ s^{-1}, the Redhead equations indicate that the desorption activation energy or adsorption energy for H_2O in the strongly adsorbed residual layer is E > 20 kcal/mol.

This estimate for the adsorption energy for H_2O in the strongly adsorbed residual layer is consistent with the previously measured kinetics for H_2O desorption from hydroxylated SiO_2 surfaces.[9] Based on laser-induced thermal

https://doi.org/10.1021/acs.jpcc.4c06859
J. Phys. Chem. C 2025, 129, 1666−1677

desorption (LITD) experiments using $H_2{}^{16}O$ and $H_2{}^{18}O$, the activation energy and preexponential for H_2O desorption were obtained at different H_2O coverages.[9] The activation energy for H_2O desorption approaches $E \sim 20$ kcal/mol for small H_2O coverages close to $\Theta \sim 0$.[9]

ATR-IR measurements of the isosteric heat of adsorption for H_2O on hydroxylated SiO_2 surface also reveal high H_2O adsorption energies at low H_2O thicknesses.[11] The adsorption energy increases progressively for H_2O thicknesses <10 Å.[11] The adsorption energy increases to ~14 kcal/mol at ~1.5 Å. The H_2O adsorption energy could easily be expected to reach 20 kcal/mol at $\Theta \sim 0$.

In contrast, the BET modeling of H_2O adsorption on SiO_2 particles obtains c values that yield an H_2O adsorption energy in the first layer that is much lower than 20 kcal/mol.[37] The H_2O adsorption energy in the first layer on SiO_2 particles is determined to be 12.0 kcal/mol from the BET modeling.[37] This adsorption energy is only nominally higher than the enthalpy of condensation of H_2O vapor of 10.5 kcal/mol.[37] This discrepancy may result from the presence of the strongly adsorbed H_2O layer on the hydroxylated SiO_2 particles prior to the various measurements. Since these SiO_2 particle measurements are based on differences and did not begin with an anneal to $T \geq 120$ °C to remove the strongly adsorbed H_2O layer, they may not be able to detect the strongly adsorbed layer.

There are several explanations for the high H_2O adsorption energy in the "ice-like" vicinal layer on hydroxylated SiO_2. Calculations have shown that H_2O forms a well-ordered and stable hydrogen-bonded network on the (100) surface of β-cristobalite described as ice tessellation.[42] In agreement with the current studies, molecular dynamics simulations indicate that this network is stable up to room temperature.[42] Near-infrared evanescent-wave cavity ring-down absorption spectroscopy has also identified an ordered H_2O monolayer in the first monolayer on hydroxylated SiO_2 consistent with a quasicrystalline network.[43] The SiOH silanol species on the hydroxylated SiO_2 surface are also acidic.[44] Proton transfer from the SiOH species to H_2O may create SiO^- H_3O^+ ion pairs that may be more strongly bound in the first monolayer.[9] Subsequent monolayers have a lower adsorption energy because they are only bound by hydrogen bonding.

At higher H_2O coverages, the desorption activation energy determined from the LITD measurements decreases with H_2O coverage.[9] The desorption activation energy reaches $E \sim 13$ kcal/mol at a H_2O coverage of 0.4 ML. This desorption activation energy is close to the measured activation energy for desorption of H_2O from ice multilayers of 11.9,[32] 13.9,[45] and 11.5 kcal/mol.[46] These desorption energies are all slightly higher than the heat of vaporization of H_2O from liquid water of 9.7 kcal/mol. The adsorption energy for H_2O in the weakly adsorbed layer on hydroxylated SiO_2 should be close to these previous measurements from ice multilayers or liquid water.

The results in Figures 5, 8 and 10 for the H_2O thickness versus H_2O pressure can also be compared with predictions for the H_2O coverage on hydroxylated SiO_2 from the H_2O adsorption and desorption kinetics.[9] These predictions use the measured H_2O desorption kinetics from hydroxylated SiO_2 given by $d\Theta/dt = -\nu_1(\Theta) \exp[-E_d(\Theta)/RT]$ where $\nu_1(\Theta) = \exp(43.4 - 7.1\Theta - 37.5\Theta^2)$ and $E(\Theta) = 21.3-15.4\Theta^{1/2}$ kcal/mol.[9] This equation for $E(\Theta)$ is valid for H_2O coverages up to 0.4 ML.[9]

These predictions for the H_2O coverage also use a reported H_2O sticking coefficient given by $S(\Theta) = 1 - 0.73\exp(-21\Theta)$.[9] This sticking coefficient becomes $S = 1$ for H_2O multilayers of water or ice.[32,46] Although the H_2O desorption kinetics are only applicable up to 0.4 ML, the predicted H_2O coverages expected from the adsorption and desorption kinetics are in approximate agreement with the strongly adsorbed H_2O coverages measured in Figures 5, 8 and 10. The predicted H_2O coverages are in the range of 0.1−0.4 ML at H_2O pressures from 0.1−5 Torr at temperatures from 18.1 to 30.4 °C employed in this investigation.

Higher H_2O pressures will lead to H_2O multilayer adsorption. The coverage-dependent desorption activation barrier is expected to level off at a value of $E \sim 10-12$ kcal/mol in the H_2O multilayer. The results in Figures 4, 7 and 9 indicate that the H_2O multilayer is not stable when the H_2O pressures are removed at 18.1, 27.2, and 30.4 °C. This instability is consistent with the desorption kinetics and residence times expected for H_2O on the surface of the H_2O multilayer. Based on estimates using eq 1, the H_2O desorption rate from the top monolayer of the H_2O multilayer is 1.58×10^4 ML/s assuming a desorption activation barrier of 12 kcal/mol, a desorption preexponential of 1×10^{13} s^{-1}, and a temperature of 25 °C. The inverse of this desorption rate is a H_2O residence time of only 6×10^{-5} s/ML. The H_2O multilayer will not be stable in the absence of the higher H_2O pressures.

III.VI. Dependence of H_2O Layer Thickness on Decreasing H_2O Pressure and Purge Time. The H_2O pressures employed in Figure 4 were also employed in descending order to determine the effect on the H_2O layer thicknesses at a stage temperature of 30.4 °C. In Figure S4a, Supporting Information, the highest pressure of 25 Torr was dosed 3 times to form the strongly adsorbed layer on the hydroxylated SiO_2 surface. The purge time for Argon was 10 min. The strongly adsorbed layer increased in thickness during the first two H_2O exposures of 25 Torr before reaching saturation by the third H_2O exposure. Then the H_2O pressures were decreased in a reverse order compared with Figure 4. Figure S4a, Supporting Information, shows that the weakly adsorbed H_2O layer thicknesses for the various H_2O pressures were the same as in Figure 4 after the third H_2O exposure of 25 Torr. This third H_2O exposure at 25 Torr saturated the weakly adsorbed H_2O layer thickness. The strongly adsorbed layer thickness remained constant during the H_2O exposures at progressively lower H_2O pressures.

Experiments also explored the effect of the purge time on the strongly adsorbed H_2O layer at a stage temperature of 30.4 °C. Figure S4b, Supporting Information, displays additional investigations at longer purge times of 100 min. These results reveal that the strongly adsorbed layer cannot be removed by a longer purge. These results further confirm the H_2O adsorption energy $E > 20$ kcal/mol. In addition, the H_2O_2 plasma procedure used to clean the initial SiO_2 surfaces was also exposed to a hydroxylated SiO_2 surface containing the saturated strongly adsorbed layer. After the H_2O_2 plasma exposure, the H_2O layer thickness was identical to the saturated strongly adsorbed layer thickness.

III.VII. Dependence of H_2O Layer Thickness on Evacuation Time and Annealing Temperature. The H_2O layer thickness on hydroxylated SiO_2 nanoparticles is slowly desorbed versus evacuation time at 25 °C after a H_2O exposure at 1 Torr/1 min. Figure 11a shows the initial

https://doi.org/10.1021/acs.jpcc.4c06859
J. Phys. Chem. C 2025, 129, 1666−1677

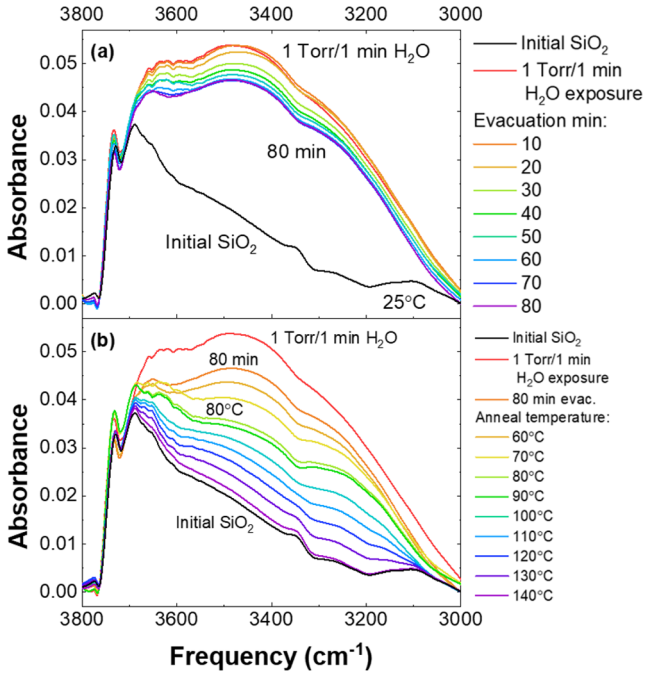

Figure 11. (a) IR absorbance from initial SiO_2 particles, after H_2O exposure at 1 Torr/1 min, and then after various evacuation times. (b) IR absorbance from initial SiO_2 particles, after H_2O exposure at 1 Torr/1 min, and then after various annealing temperatures. Absorbance from any gas phase H_2O has been removed from the spectra.

hydroxylated SiO_2 surface, the hydroxylated SiO_2 surface immediately after a 1 Torr/1 min H_2O exposure, and then the hydroxylated SiO_2 surface after evacuation for a variety of evacuation times at 25 °C. The absorbance from any gas phase H_2O has again been subtracted from the spectra in Figure 11a. The H_2O layer is slowly desorbed under vacuum at 25 °C. However, there is a strongly adsorbed H_2O layer that remains after an 80 min evacuation. These results are consistent with the H_2O layer thickness results after removing the H_2O pressure shown in Figures 4, 7 and 9.

Experiments were also performed by heating the hydroxylated SiO_2 nanoparticles to determine the stability of the strongly adsorbed H_2O layer. Figure 11b shows FTIR spectra of the initial hydroxylated SiO_2 nanoparticles, the hydroxylated SiO_2 nanoparticles immediately after a 1 Torr/1 min H_2O exposure, the hydroxylated SiO_2 nanoparticles after evacuation for 80 min, and then after annealing to a variety of temperatures from 60 to 140 °C under vacuum. The absorbance from any gas phase H_2O has been removed from the spectra in Figure 11b. The spectrum after annealing to 140 °C is equivalent to the initial hydroxylated SiO_2 nanoparticles. This behavior indicates that all the adsorbed H_2O has been desorbed by annealing to 140 °C.

The FTIR spectra in Figure 11b display a progressive loss of absorbance for the O−H stretching vibrations of adsorbed H_2O versus annealing temperature. There is minimal absorbance loss from recombinative desorption after annealing to 140 °C. SiOH surface hydroxyl species are just beginning to be lost resulting from recombinative desorption (2SiOH → SiOSi + H_2O) at 140 °C.[18] The SiOH surface hydroxyl species are lost slowly with annealing and are not completely removed until annealing temperatures of 1000 °C.[18]

The strongly adsorbed H_2O layer thickness on hydroxylated SiO_2 versus annealing was also measured using spectroscopic ellipsometry. In these experiments, the SiO_2 samples were heated to a stage temperature of 124 °C and cleaned with H_2O_2 plasma for 30 s. The samples were then cooled down to a stage temperatures of 30.4 °C and then exposed to H_2O to saturate the strongly adsorbed layer. The H_2O exposure consisted of three 30 min, 25 Torr static water exposures separated by Ar purging for 10 min. There was ∼0.8 Å of strongly adsorbed H_2O on the hydroxylated SiO_2 surface after these H_2O exposures. The sample was then heated to a specified annealing temperature and held at that annealing temperature for 1 h. Following the annealing, the chamber was cooled to a stage temperature of 30.4 °C and the H_2O layer thickness was measured with ellipsometry.

Figure 12a shows the H_2O layer thickness before annealing and after annealing for eight SiO_2 samples for annealing stage

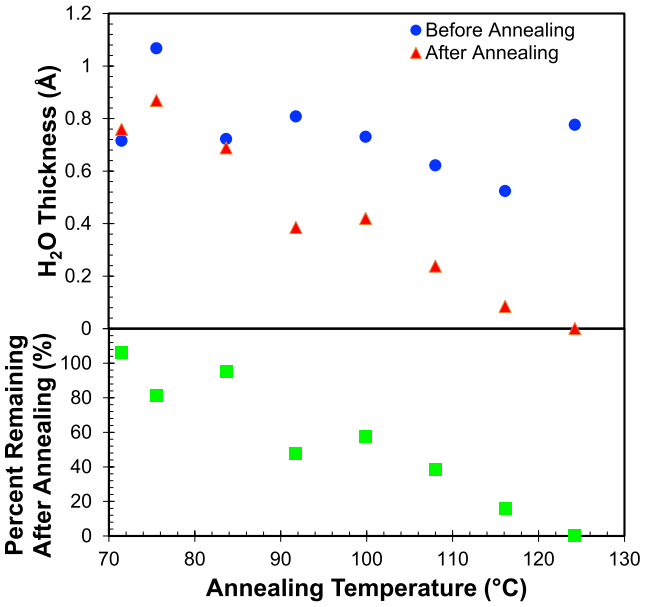

Figure 12. (a) Strongly adsorbed H_2O layer thickness before and after annealing to various stage temperatures. (b) Percentage of strongly adsorbed layer remaining after annealing to various stage temperatures.

temperatures from 72 to 124 °C. The H_2O layer thickness is progressively reduced over this temperature range. The thicknesses of the H_2O layer before and after annealing were then employed to calculate the percentage of the H_2O layer remaining after annealing. These results in Figure 12b reveal that there is a nearly linear reduction in the strongly adsorbed H_2O layer thickness for annealing stage temperatures from 72 to 124 °C. These results are in good agreement with the FTIR results for the change in absorbance versus annealing from 60 to 140 °C displayed in Figure 11b.

IV. CONCLUSIONS

The H_2O layer on flat hydroxylated SiO_2 surfaces and SiO_2 nanoparticles was examined in vacuum using spectroscopic ellipsometry (SE) and Fourier transform infrared (FTIR) spectroscopy. The SE measurements monitored H_2O layer thicknesses versus H_2O pressure at various temperatures. The H_2O pressures were varied up to the saturation H_2O vapor pressure corresponding to the sample temperature. The FTIR

https://doi.org/10.1021/acs.jpcc.4c06859
J. Phys. Chem. C 2025, 129, 1666−1677

measurements detected the H_2O layer using the O−H stretching vibration for H_2O. Both the SE and FTIR measurements revealed that the H_2O layer grew versus H_2O pressure at temperatures from 18.1 to 30.4 °C. There was also a H_2O layer remaining on the SiO_2 surface after removing the H_2O pressure.

The SE measurements revealed that there were two types of H_2O layers: a thin strongly adsorbed layer and a weakly adsorbed layer that was much thicker at high H_2O pressures. The strongly adsorbed layer was not lost by removing the H_2O pressure. However, the strongly adsorbed layer could be desorbed by heating the sample stage to 124 °C. The weakly adsorbed layer could be added or subtracted by increasing or decreasing the H_2O pressure. The FTIR measurements confirmed the presence of the two types of H_2O layers.

The SE measurements characterized the layer thicknesses for the strongly and weakly adsorbed layers versus H_2O pressure at 18.1, 27.2, and 30.4 °C. Using repeating H_2O exposures, the thin strongly adsorbed layer reached an approximate plateau at ∼1 Å at the various temperatures. Based on the stability of the strongly adsorbed H_2O layer, this layer was consistent with an adsorption energy of >20 kcal/mol based on the Redhead equations for desorption. Other studies have characterized this vicinal layer as an "ice-like" layer composed of a crystalline orientation in the first monolayer.

In contrast to the thin strongly adsorbed H_2O layer, the weakly adsorbed layer obtained much higher multilayer H_2O thicknesses at larger H_2O pressures. For example, the weakly adsorbed multilayer thickness was 7.5 Å at 92% relative humidity at 30.4 °C (30 Torr). The weakly adsorbed layer has characteristics that resemble multilayer adsorption curves expected from the BET model. The weakly adsorbed layer is believed to be more "liquid-like" with an adsorption energy of ∼12 kcal/mol similar to the desorption energy for H_2O from ice or water multilayers.

The SE and FTIR investigations confirmed that the strongly adsorbed H_2O layer was stable at temperatures from 18.1 to 30.4 °C for purge times as long as 100 min and evacuation times as long as 80 min, respectively. The SE and FTIR studies also revealed that the strongly adsorbed H_2O layer was not completely lost until reaching annealing temperatures of 124−140 °C. These studies confirm the existence of a thin strongly adsorbed vicinal H_2O layer on hydroxylated SiO_2 surfaces and a weakly adsorbed H_2O layer on top of the vicinal layer that is dependent on H_2O pressure and is only present under H_2O exposure.

■ ASSOCIATED CONTENT

Supporting Information

The Supporting Information is available free of charge at https://pubs.acs.org/doi/10.1021/acs.jpcc.4c06859.

Schematic of experimental chamber; temperature calibration of sample stage; water contact angles for SiO_2 surfaces; and H_2O layer thicknesses for H_2O pressures that decrease versus time and for longer purge times (PDF)

■ AUTHOR INFORMATION

Corresponding Author

Steven M. George − *Department of Chemistry, University of Colorado, Boulder, Colorado 80309, United States;* orcid.org/0000-0003-0253-9184; Phone: 303-492-3398; Email: Steven.George@Colorado.edu

Authors

Samantha M. Rau − *Department of Chemistry, University of Colorado, Boulder, Colorado 80309, United States*

Rebecca J. Hirsch − *Department of Chemistry, University of Colorado, Boulder, Colorado 80309, United States*

Marcel Junige − *Department of Chemistry, University of Colorado, Boulder, Colorado 80309, United States;* orcid.org/0000-0002-6633-2759

Andrew S. Cavanagh − *Department of Chemistry, University of Colorado, Boulder, Colorado 80309, United States;* orcid.org/0000-0002-6201-530X

Antonio L. P. Rotondaro − *Tokyo Electron America, Inc, Austin, Texas 78741, United States*

Hanna Paddubrouskaya − *Tokyo Electron America, Inc, Austin, Texas 78741, United States*

Kate H. Abel − *Tokyo Electron America, Inc, Austin, Texas 78741, United States*

Complete contact information is available at: https://pubs.acs.org/10.1021/acs.jpcc.4c06859

Notes

The authors declare no competing financial interest.

■ ACKNOWLEDGMENTS

This work was funded by Tokyo Electron America, Inc (TEL). TMEiC provided the O_3 generator. The authors would like to thank Kenneth Smith for the design and fabrication of the V-shaped chamber with cooled stage used for the ellipsometry experiments.

■ REFERENCES

(1) Björnehohn, E.; Hansen, M. H.; Hodgson, A.; Liu, L. M.; Limmer, D. T.; Michaelides, A.; Pedevilla, P.; Rossmeisl, J.; Shen, H.; Tocci, G.; et al. Water at Interfaces. *Chem. Rev.* **2016**, *116*, 7698−7726.

(2) Ewing, G. E. Ambient Thin Film Water on Insulator Surfaces. *Chem. Rev.* **2006**, *106*, 1511−1526.

(3) Tang, M. J.; Cziczo, D. J.; Grassian, V. H. Interactions of Water with Mineral Dust Aerosol: Water Adsorption, Hygroscopicity, Cloud Condensation, and Ice Nucleation. *Chem. Rev.* **2016**, *116*, 4205−4259.

(4) Henderson, M. A. The Interaction of Water With Solid Surfaces: Fundamental Aspects Revisited. *Surf. Sci. Rep.* **2002**, *46*, 1−308.

(5) Thiel, P. A.; Madey, T. E. The Interaction of Water With Solid-Surfaces - Fundamental-Aspects. *Surf. Sci. Rep.* **1987**, *7*, 211−385.

(6) Zhuravlev, L. T. The Surface Chemistry of Amorphous Silica. Zhuravlev Model. *Colloids Surf., A* **2000**, *173*, 1−38.

(7) Asay, D. B.; Kim, S. H. Evolution of the Adsorbed Water Layer Structure on Silicon Oxide at Room Temperature. *J. Phys. Chem. B* **2005**, *109*, 16760−16763.

(8) Chen, L.; He, X.; Liu, H. S.; Qian, L. M.; Kim, S. H. Water Adsorption on Hydrophilic and Hydrophobic Surfaces of Silicon. *J. Phys. Chem. C* **2018**, *122*, 11385−11391.

(9) Sneh, O.; Cameron, M. A.; George, S. M. Adsorption and Desorption Kinetics of H_2O on a Fully Hydroxylated SiO_2 Surface. *Surf. Sci. Rep.* **1996**, *364*, 61−78.

(10) Verdaguer, A.; Weis, C.; Oncins, G.; Ketteler, G.; Bluhm, H.; Salmeron, M. Growth and Structure of Water on SiO_2 Films on Si Investigated by Kelvin Probe Microscopy and In Situ X-Ray Spectroscopies. *Langmuir* **2007**, *23*, 9699−9703.

(11) Asay, D. B.; Barnette, A. L.; Kim, S. H. Effects of Surface Chemistry on Structure and Thermodynamics of Water Layers at Solid-Vapor Interfaces. *J. Phys. Chem. C* **2009**, *113*, 2128−2133.
(12) Sumner, A. L.; Menke, E. J.; Dubowski, Y.; Newberg, J. T.; Penner, R. M.; Hemminger, J. C.; Wingen, L. M.; Brauers, T.; Finlayson-Pitts, B. J. The Nature of Water on Surfaces of Laboratory Systems and Implications for Heterogeneous Chemistry in the Troposphere. *Phys. Chem. Chem. Phys.* **2004**, *6*, 604−613.
(13) Beaglehole, D.; Christenson, H. K. Vapor Adsorption on Mica and Silicon - Entropy Effects, Layering, and Surface Forces. *J. Phys. Chem. A* **1992**, *96*, 3395−3403.
(14) Chen, J.; Ratera, I.; Park, J. Y.; Salmeron, M. Velocity Dependence of Friction and Hydrogen Bonding Effects. *Phys. Rev. Lett.* **2006**, *96*, No. 236102.
(15) Williams, K. R.; Muller, R. S. Etch Rates for Micromachining Processing. *J. Microelectromech. Syst.* **1996**, *5*, 256−269.
(16) Helms, C. R.; Deal, B. E. Mechanisms of the HF/H_2O Vapor Phase Etching of SiO_2. *J. Vac. Sci. Technol., A* **1992**, *10*, 806−811.
(17) Bluhm, H. Photoelectron Spectroscopy of Surfaces under Humid Conditions. *J. Electron Spectrosc. Relat. Phenom.* **2010**, *177*, 71−84.
(18) Sneh, O.; George, S. M. Thermal Stability of Hydroxyl Groups on a Well-Defined Silica Surface. *J. Phys. Chem. A* **1995**, *99*, 4639−4647.
(19) McCrackin, F. L.; Passaglia, E.; Stromberg, R. R.; Steinberg, H. L. Measurement of Thickness and Refractive Index of Very Thin Films and Optical Properties of Surfaces by Ellipsometry. *J. Res. Natl. Bur. Stand., Sect. A* **1963**, *67A*, 363−377.
(20) Synowicki, R. A.; Pribil, G. K.; Cooney, G.; Herzinger, C. M.; Green, S. E.; French, R. H.; Yang, M. K.; Burnett, J. H.; Kaplan, S. Fluid Refractive Index Measurements Using Rough Surface and Prism Minimum Deviation Techniques. *J. Vac. Sci. Technol., B* **2004**, *22*, 3450−3453.
(21) Hale, G. M.; Querry, M. R. Optical Constants of Water in 200-nm to 200-mm Wavelength Region. *Appl. Opt.* **1973**, *12*, 555−563.
(22) Essen, L. The Refractive Indices of Water Vapour, Air, Oxygen, Nitrogen, Hydrogen, Deuterium and Helium. *Proc. Phys. Soc. B* **1953**, *66*, 189−193.
(23) Herzinger, C. M.; Johs, B.; McGahan, W. A.; Woollam, J. A.; Paulson, W. Ellipsometric Determination of Optical Constants for Silicon and Thermally Grown Silicon Dioxide via a Multi-Sample, Multi-Wavelength, Multi-Angle Investigation. *J. Appl. Phys.* **1998**, *83*, 3323−3336.
(24) Jellison, G. E.; Modine, F. A. Optical Functions of Silicon Between 1.7 and 4.7 eV at Elevated-Temperatures. *Phys. Rev. B* **1983**, *27*, 7466−7472.
(25) Jellison, G. E.; Modine, F. A. Optical Functions of Silicon at Elevated-Temperatures. *J. Appl. Phys.* **1994**, *76*, 3758−3761.
(26) Junige, M.; George, S. M. Area-Selective Molecular Layer Deposition of Nylon 6,2 Polyamide: Growth on Carbon and Inhibition on Silica. *J. Vac. Sci. Technol., A* **2021**, *39*, No. 023204.
(27) Hilfiker, J. N.; Singh, N.; Tiwald, T.; Convey, D.; Smith, S. M.; Baker, J. H.; Tompkins, H. G. Survey of Methods to Characterize Thin Absorbing Films with Spectroscopic Ellipsometry. *Thin Solid Films* **2008**, *516*, 7979−7989.
(28) Petrenko, V. F.; Whitworth, R. W. *Physics of Ice*; Oxford University Press: Oxford and New York, 1999.
(29) DuMont, J. W.; George, S. M. Pyrolysis of Alucone Molecular Layer Deposition Films Studied Using In Situ Transmission Fourier Transform Infrared Spectroscopy. *J. Phys. Chem. C* **2015**, *119*, 14603−14612.
(30) Ballinger, T. H.; Wong, J. C. S.; Yates, J. T. Transmission Infrared-Spectroscopy of High Area Solid-Surfaces - A Useful Method for Sample Preparation. *Langmuir* **1992**, *8*, 1676−1678.
(31) Ferguson, J. D.; Weimer, A. W.; George, S. M. Atomic Layer Deposition of Ultrathin and Conformal Al_2O_3 Films on BN Particles. *Thin Solid Films* **2000**, *371*, 95−104.
(32) Haynes, D. R.; Tro, N. J.; George, S. M. Condensation and Evaporation of H_2O on Ice Surfaces. *J. Phys. Chem. A* **1992**, *96*, 8502−8509.
(33) George, S. M.; Livingston, F. E. Dynamic Ice Surface in the Polar Stratosphere. *Surf. Rev. Lett.* **1997**, *04*, 771−780.
(34) Wallace, W. E. *NIST Chemistry WebBook, SRD 69, Water*, NIST Mass Spectrometry Data Center.
(35) Eisenberg, D.; Kauzmann, W. *The Structure and Properties of Water*; Oxford University Press: New York and Oxford, 1969.
(36) Brunauer, S.; Emmett, P. H.; Teller, E. Adsorption of Gases in Multimolecular Layers. *J. Am. Chem. Soc.* **1938**, *60*, 309−319.
(37) Goodman, A. L.; Bernard, E. T.; Grassian, V. H. Spectroscopic Study of Nitric Acid and Water Adsorption on Oxide Particles: Enhanced Nitric Acid Uptake Kinetics in the Presence of Adsorbed Water. *J. Phys. Chem. A* **2001**, *105*, 6443−6457.
(38) Keskinen, H.; Romakkaniemi, S.; Jaatinen, A.; Miettinen, P.; Saukko, E.; Joutsensaari, J.; Mäkelä, J. M.; Virtanen, A.; Smith, J. N.; Laaksonen, A. On-Line Characterization of Morphology and Water Adsorption on Fumed Silica Nanoparticles. *Aerosol Sci. Technol.* **2011**, *45*, 1441−1447.
(39) Ma, Q. X.; He, H.; Liu, Y. C. In Situ Drifts Study of Hygroscopic Behavior of Mineral Aerosol. *J. Environ. Sci.* **2010**, *22*, 555−560.
(40) Schuttlefield, J.; Al-Hosney, H.; Zachariah, A.; Grassian, V. H. Attenuated Total Reflection Fourier Transform Infrared Spectroscopy to Investigate Water Uptake and Phase Transitions in Atmospherically Relevant Particles. *Appl. Spectrosc.* **2007**, *61*, 283−292.
(41) Redhead, P. A. Thermal Desorption of Gases. *Vacuum* **1962**, *12*, 203−211.
(42) Yang, J. J.; Meng, S.; Xu, L. F.; Wang, E. G. Ice Tessellation on a Hydroxylated Silica Surface. *Phys. Rev. Lett.* **2004**, *92*, No. 146102.
(43) Aarts, I. M. P.; Pipino, A. C. R.; Hoefnagels, J. P. M.; Kessels, W. M. M.; van de Sanden, M. C. M. Quasi-Ice Monolayer on Atomically Smooth Amorphous SiO_2 at Room Temperature Observed with a High-Finesse Optical Resonator. *Phys. Rev. Lett.* **2005**, *95*, No. 166104.
(44) Parks, G. A. Isoelectric Points of Solid Oxides Solid Hydroxides and Aqueous Hydroxo Complex Systems. *Chem. Rev.* **1965**, *65*, 177−198.
(45) Smith, J. A.; Livingston, F. E.; George, S. M. Isothermal Desorption Kinetics of Crystalline H_2O, $H_2{}^{18}O$, and D_2O Ice Multilayers. *J. Phys. Chem. B* **2003**, *107*, 3871−3877.
(46) Brown, D. E.; George, S. M.; Huang, C.; Wong, E. K. L.; Rider, K. B.; Smith, R. S.; Kay, B. D. H_2O Condensation Coefficient and Refractive Index for Vapor-Deposited Ice from Molecular Beam and Optical Interference Measurements. *J. Phys. Chem. A* **1996**, *100*, 4988−4995.

https://doi.org/10.1021/acs.jpcc.4c06859
J. Phys. Chem. C 2025, 129, 1666−1677